Check for updates

ChemPlusChem
Research Article
doi.org/10.1002/cplu.202400073
Chemistry Europe
European Chemical Societies Publishing
www.chempluschem.org

Transparent Conductive Titanium and Fluorine Co-doped Zinc Oxide Films

Iqra Ramzan,[a] Joanna Borowiec,[a] Ivan P. Parkin,[a] and Claire J. Carmalt*[a]

Aerosol-assisted chemical vapor deposition (AACVD) was used to deposit highly transparent and conductive titanium or fluorine-doped and titanium-fluorine co-doped ZnO thin films on glass substrate at 450 °C. All films were characterized by X-ray photoelectron spectroscopy (XPS), X-ray diffraction (XRD), UV-Vis spectroscopy, scanning electron spectroscopy (SEM), and four-point probe. The films were 600–680 nm thick, crystalline, and highly transparent (80–87 %). The co-doped film consisted of 0.70 at% titanium and 1 at% fluorine, and displayed a charger carrier mobility, charge carrier concentration, and a minimum resistivity of 8.4 $cm^2 V^{-1} s^{-1}$, 3.97×10^{20} cm^{-3}, and 1.69×10^{-3} Ωcm, respectively. A band gap of 3.6 eV was observed for the co-doped film. Compared to the undoped and singly doped films, the co-doped film displayed a notably higher structure morphology (more homogenous grains with well-defined boundaries) suitable for transparent conducting oxide applications.

Introduction

Transparent conductive oxides (TCOs) have long been used as imperative components in optoelectronic devices, and their applications are constantly expanding.[1] TCOs are best characterized by their transparency, which exceeds 80 % in the visible spectrum, their band gap above 3.1 eV, and their electrical resistivity values no higher than 10^{-3} Ωcm.[2] Consequently, they qualify as optically transparent materials with reasonably high electrical conductance. The high electrical conductivity is an outcome of the number of free charge carriers and their resulting mobility.[2,3] Achieving transparency and conductivity together is mutually exclusive because transparency relies on a wide band gap which could otherwise impede the production of charge carriers, hence a compromise between these two properties is unavoidable. This conundrum can be sidestepped by introducing dopant into the material to enable the formation of charge carriers in order to increase conductivity.[4] Doping is also crucial as it can alter the band gap of semiconductors, it can widen or narrow the band gap noticeably at high concentrations of doping.[5–7] However, excessive doping is not favorable since it can negatively impact conductivity by deteriorating the film structure, resulting in decreasing the mobility of free charge carriers.[8–11]

The present industrial standard and most produced TCO is indium doped tin oxide (ITO), followed by fluorine doped tin oxide (FTO).[12] Both commercially available TCOs, namely ITO and FTO, have low resistivity (10^{-4} Ωcm) and high optical transmittance (> 85 %). However, the limited availability and unpredictable price of indium, and increased price of tin over the last few years pose challenges in the present competitive market. Therefore, there is a demand for new low-cost, highly abundant TCO materials as an alternative to available expensive TCOs or to improve their properties. Zinc oxide (ZnO) has generated substantial research interest due to its distinct advantages, such as optical and electrical properties comparable to ITO, large excitation binding energy, non-toxicity, easy preparation, stability in plasma[13] and most importantly its natural abundance.

ZnO with the wurtzite structure is a semiconductor with a wide band gap (~3.3 eV).[14] However, pure ZnO has high electrical resistivity which limits its applications. The introduction of dopants into the lattice of ZnO is recognized to modify its properties. Al,[11,15,16] Ga,[17] Mo,[18,19] P,[20] Si,[9] Sc,[10] Y,[21] B,[22] Ti,[23] Cl,[24] and F[25] have been reported as dopants to enhance the conductivity and transparency of ZnO. For instance, fluorine (F^-) by substituting O^{2-} gets incorporated into the ZnO lattice, inducing one extra free electron, is highly suitable dopant for achieving n-type conductivity. Group IV elements as dopants for ZnO have also received much attention.[9,10,23]

Ti is chosen as a cationic dopant for this study due to its ability to produce more free charges per dopant atom, its widely reported excellent electrical and optical properties,[26–29] and suitability for a variety of optoelectronic applications such as electrodes. Ti-doped ZnO (TZO) exhibited higher work function than most widely researched AZO (aluminum doped zinc oxide), and emerges as a superior option to act as an anode in organic light emitting diode (OLED) devices compared to AZO and even ITO.[30,31] However, the dopant window of Ti impurity is very small because excessive Ti-ions can act as scattering centers and thus enhance the resistivity.[32] This led us to add a potential co-dopant to achieve higher electrical conductivity. F was chosen as a co-dopant due to the

[a] I. Ramzan, J. Borowiec, I. P. Parkin, C. J. Carmalt
Materials Chemistry Centre, Department of Chemistry,
University College London,
London WC1H 0AJ (UK)
E-mail: c.j.carmalt@ucl.ac.uk

Supporting information for this article is available on the WWW under https://doi.org/10.1002/cplu.202400073

© 2024 The Authors. ChemPlusChem published by Wiley-VCH GmbH. This is an open access article under the terms of the Creative Commons Attribution License, which permits use, distribution and reproduction in any medium, provided the original work is properly cited.

21926506, 0, Downloaded from https://chemistry-europe.onlinelibrary.wiley.com/doi/10.1002/cplu.202400073 by University College London UCL Library Services, Wiley Online Library on [09/05/2024]. See the Terms and Conditions (https://onlinelibrary.wiley.com/terms-and-conditions) on Wiley Online Library for rules of use; OA articles are governed by the applicable Creative Commons License

similarities in ionic sizes of F^- and O^{2-} (O^{2-}: 1.24 Å; F^-: 1.17 Å), lower lattice distortion, and stable bonding due to high electronegativity. Furthermore, the electronic disturbance of F-doped ZnO (FZO) films is predominantly limited to the valence band and thus reduces the scattering of free carriers.[33,34] This indicates that F along with Ti as dopants can greatly stabilize the ZnO thin films and help to achieve desired optoelectronic properties.

Several methods have been utilized for the fabrication of ZnO thin films, comprising sputtering,[23] spray pyrolysis,[35] sol-gel,[36] and chemical vapour deposition (CVD).[37] This research centers on ZnO thin films, undoped-ZnO, Ti:ZnO (TZO), F:ZnO (FZO), and uniquely Ti:F:ZnO (TFZO), deposited using aerosol-assisted CVD (AACVD). AACVD has significant edge over conventionally used CVD methods in term of precursors not necessarily required to be thermally stable, or volatile, which can be employed at atmospheric pressure, and is an affordably low-cost technique for the large-scale production of thin films.[38–40] In this work, we show that co-doping (TFZO) improves the optical and electrical properties of the AACVD undoped ZnO film.

Experimental Section

The following chemicals were purchased from Sigma Aldrich: anhydrous zinc acetate (99.99%), ammonium fluoride (98%), titanium butoxide (98%). Methanol (99.9%) and acetic acid (99%) were supplied by Fisher Scientific. All the chemicals were used as received without any further purification.

A typical precursor solution was prepared by dissolving anhydrous zinc acetate (0.2 g, 0.00109 mol) in methanol (20 mL), followed by adding a dopant. Films doped with fluorine were deposited by adding 0.0005 g (1.31 mole% with respect to zinc acetate) of ammonium fluoride to zinc acetate solution, but when doping with titanium, titanium butoxide (4 uL, 1.16 mole% with respect to zinc acetate) was added to zinc acetate solution. For co-doping, both dopants were added to the zinc acetate solution at the same time in a given ratio. Approximately 1 mL of acetic acid was added to achieve higher solubility of precursors. Before transferring to the gas bubbler, the precursor solution was stirred for 15 minutes. A standard float glass substrate plate (15 cm×5 cm×0.3 cm) with 50 nm thick SiO_2 ion-diffusion inhibiting layer coated on the top surface was supplied by Pilkington's NSG (Wigan, Lancashire, UK). The SiO_2 layer acted as a barrier to prevent leaching of ions between the deposited film and substrate. A horizontal bed AACVD reactor was used, the glass substrate was horizontally placed on a smooth graphite heating block with a top plate suspended above 0.5 cm, housed inside a quartz tube. The top plate ensured the laminar flow of aerosol to enable uniform deposition. The substrate was heated to 450 °C and depositions were performed under the flow (1.0 L min^{-1}) of N_2 as carrier gas. The precursor solution was nebulized using a piezo ultrasonic atomizer from Johnson Matthey, which operates at a frequency of 1.6 MHz to generate a mode droplet size of 3 mm.

The generated aerosol mist of precursor solution was transported by a carrier N_2 gas into the deposition chamber. The whole set up was placed in a fume cupboard. All the precursor solution was misted in 50 ± 5 minutes to deposit the film. After the completion of deposition, the atomizer was closed, and substrate was cooled to 50 °C under the constant flow of N_2 gas.

Films Analysis

X-ray photoelectron spectroscopy (XPS) measurements of the films were performed by employing a Thermo Scientific spectrophotometer fitted with a monochromatic Al–Kα source of radiation. Chemical components were identified by performing high resolution surface scans of the C 1s, Zn 2p, O 1s, F 1s, and Ti 2p regions. These scans were recorded at the pass energy of 40 eV and a spot size of 400 μm. The peaks were identified and quantified by using Avantage Thermo Fisher scientific and plotted in OriginPro. XPS spectra were quantified to determine the dopant concentrations (at%) in ZnO films. Binding energies of the peaks were calibrated with respect to adventitious carbon peak at 284.5 eV to rectify the charging impacts.

Grazing-incident X-ray diffraction (GIXRD) patterns were recorded using Panalytical Empyrean diffractometer. Cu Kα source was used to generate the X-rays with radiation of 1.5406 Å wavelength, a voltage source of 40 kV, and an emission current of 40 mA. The angle of incident beam was kept at 1°, and the patterns were recorded from 10 to 65° (0.05° steps at 0.5°/step). Peak positions were identified by comparing them to standard data from the JCPDs card number obtained using JADE software. The patterns were interpreted to estimate crystallinity and preferred growth orientation and plotted using OriginPro.

UV-Vis transmittance and haze spectra were recorded using Shimadzu 3600i plus spectrometer over a wavelength range of 300–1500 nm. The band gap of films was calculated from acquired spectra. For haze measurements, both diffused and total transmittance were measured. Total transmittance was the sum of light transmitted through the sample and the scattered light.

Scanning electron microscopy (SEM) images were recorded to find out the films morphologies from the top-down configuration using JEOL JSM-7600 field emission (FE) instrument with an accelerating voltage of 3–5 KeV. The samples were gold coated prior to analysis to avoid charging.

Filmetrics F20 was used to determine the films thicknesses. The instrument was operated in air under reflectance mode. Hall effect measurements were carried out to record the electronic properties of films. These measurements were accomplished on an Ecopia HMS-3000 set up in the Van der Pauw configuration to measure the resistivity, mobility, sheet resistance, and carrier concentration. The samples of 1 cm^2 were used for the measurements under an input current and a calibrated magnetic field of 0.58 T. Different samples were able to pass different input currents depending on their conductivity, thus, 1 nA was set for undoped ZnO, 1 μA for singly doped films, and 1 mA for co-doped film.

Results and Discussions

Thin films of undoped ZnO, titanium-doped ZnO (TZO), fluorine-doped ZnO (FZO), and titanium-fluorine co-doped ZnO (TFZO) were fabricated on glass substrates via AACVD. The

© 2024 The Authors. ChemPlusChem published by Wiley-VCH GmbH

undoped ZnO film was deposited from the CVD reaction of zinc acetate delivered in methanol aerosol and doped/co-doped films were produced by the addition of titanium butoxide or/and ammonium fluoride in the zinc acetate solution. These commercial grade precursors decomposed cleanly and led to stable films that were very adhered to the substrate and passed the scotch tape test. A series of experiments were conducted using different amounts of dopants to determine the optimum dopants level that ensures desired optoelectronic properties. For details see Table S1 (Supporting Information). However, the experimental results focus solely on the low resistive samples. All the depositions were performed at the substrate temperature of 450 °C, as this temperature value has been widely reported to deposit conductive and transparent doped ZnO films via AACVD.[11,25,40–47]

Elemental Analysis

X-ray photoelectron spectroscopy was carried out on the surface of undoped and doped ZnO thin films to identify the oxidation states of elements. For Zn 2p scan, all the films showed two peaks associated with Zn $2p_{3/2}$ and Zn $2p_{1/2}$, as plotted in Figure 1. The undoped-ZnO film exhibited a $2p_{3/2}$ peak at 1021.3 eV, agreeing perfectly with the reported literature.[25,48] However, the doped films had a slightly shifted Zn $2p_{3/2}$ peak at 1020.98 eV, 1021.09 eV, and 1021.15 eV for TZO, FZO, and TFZO, respectively. This slight shift could be due to the introduction of dopants in the matrix of ZnO, similar results were already reported for doped ZnO films.[25]

The Ti 2p spectra of TFZO and TZO (Figure 2(a) and 2(b)) displayed Ti $2p_{3/2}$ and Ti $2p_{1/2}$ peaks. The peak attributed as Ti $2p_{3/2}$ was located at 458.49 eV and 458.53 eV for TZO and TFZO, respectively. The binding energy value of Ti $2p_{3/2}$ peak confirms that Ti was in the oxidation state of Ti^{4+}.[49] The peak fitting of the Ti 2p spectra rules out the existence of Ti^{2+} and Ti^{0}, which are typically observed to be separated by approximately 3–4 eV from the typical Ti^{4+} $2p_{3/2}$ peak position.[50] No change in Ti^{4+} phase due to co-doping was observed. The content of Ti^{4+} was found to be 1.1 at % for TZO and 0.70 at % for TFZO.

The peak located at 685.1 eV and 685 eV for TFZO and FZO as plotted in Figure 2(c) and 2(d), is a typical peak associated with F 1s.[51] This result suggested the successful inclusion of F into the lattice of ZnO. Following the analysis performed by *Nefedov et al.* on the binding energy of ZnF_2, it can be deduced that the F has replaced the O position and bonded to Zn, accomplishing the intended purpose of creating free carriers.[52] The F content was found to be 0.9 at % for FZO and 1 at % for TFZO. Depth profiling of the TFZO film (Figure 3) showed that Ti and F were not surface segregated. The concentrations of both Ti and F remained notably consistent throughout the bulk of the film.

Crystal Structure

Figure 4 shows the normalized diffraction patterns for the undoped ZnO, TZO, FZO, and TFZO. All the films showed reflections for single phase ZnO at 31.7, 34.4, 36.2, 47.5, 56.6, and 62.8 degrees assigned to (100), (002), (101), (102), (110), and (103) crystal planes, respectively. The (110) peak was

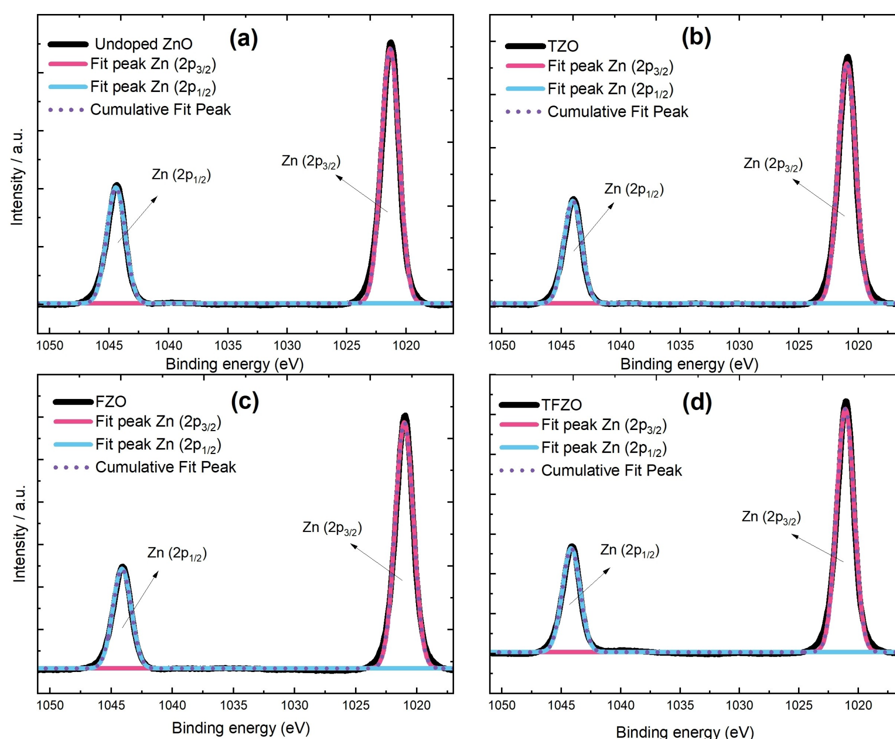

Figure 1. Zn 2p XPS spectra for undoped and doped ZnO film: (a) undoped ZnO, (b) TZO, (c) FZO, (d) TFZO.

© 2024 The Authors. ChemPlusChem published by Wiley-VCH GmbH

21926506, 0, Downloaded from https://chemistry-europe.onlinelibrary.wiley.com/doi/10.1002/cplu.202400073 by University College London UCL Library Services, Wiley Online Library on [09/05/2024]. See the Terms and Conditions (https://onlinelibrary.wiley.com/terms-and-conditions) on Wiley Online Library for rules of use; OA articles are governed by the applicable Creative Commons License

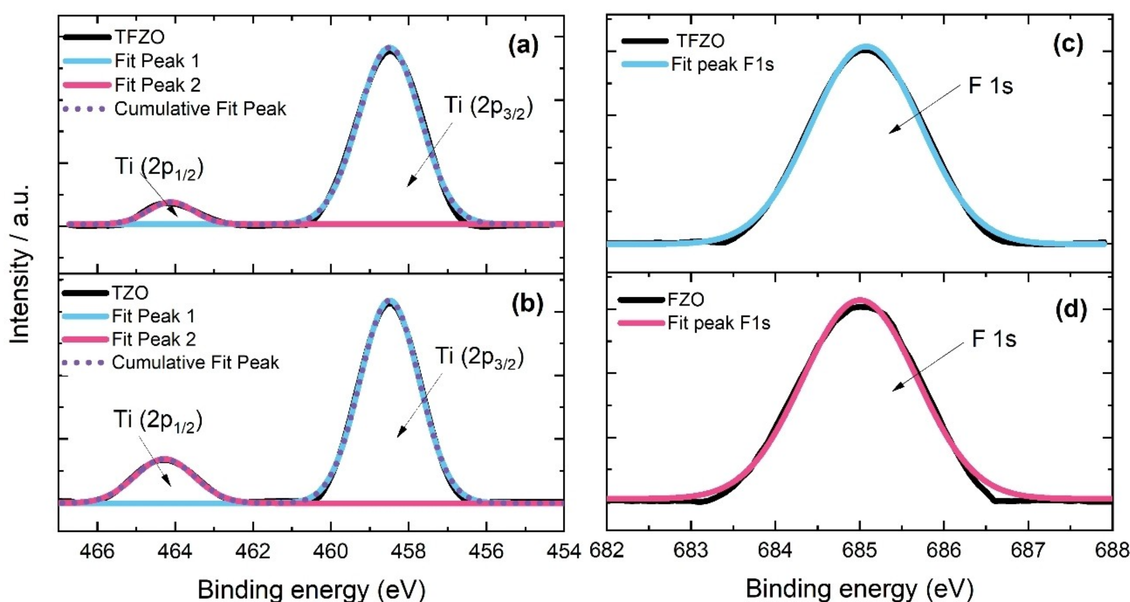

Figure 2. Ti 2p and F 1s XPS spectra for (a) Ti 2p spectra of TFZO, (b) Ti 2p spectra of TZO, (c) F 1s spectra of TFZO, and (d) F 1s spectra of FZO.

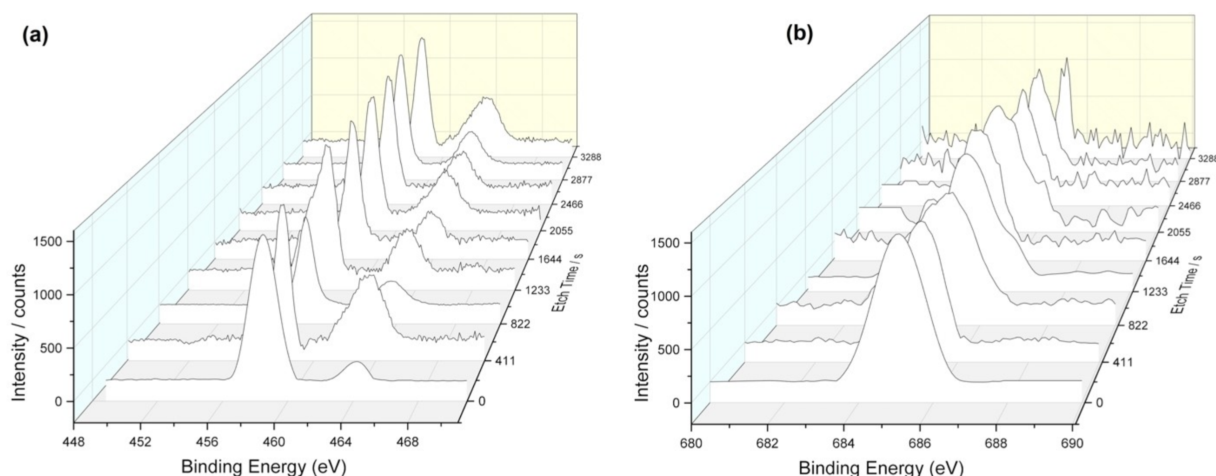

Figure 3. XPS depth profiling of the co-doped TFZO film showing (a) Ti and (b) F content as a function of etch time.

missing in the FZO thin film XRD pattern. All the listed diffraction peaks matched well with theoretical powder pattern obtained from the JCPDS card No. 70-2551 (wurtzite hexagonal structure with $a=3.249$ Å, $c=5.207$ Å). No other crystalline phases were observed. Preferred orientation was identified via texture coefficient (TC) calculations, using the Equation (1):[53]

$$TC_{hkl}=\frac{\frac{I_{meas.}(hkl)}{I_o(hkl)}}{\frac{1}{N}\sum_{h'k'l'}\frac{I_{meas.}(h'k'l')}{I_o(h'k'l')}} \tag{1}$$

Where $I_{meas.}$ is the measured intensity of individual (hkl) plane reflection, I_o is the theoretical intensity obtained from the JCPDs card, and N is the total number of reflections included in calculation, i.e., (100), (002), (101), (102), (110), and (103) peaks. The TC values listed in Table 1 indicate that all the samples exhibited preferred orientation in the (002) plane, as the crystallites preferred to pack along the *c*-direction. However, for undoped ZnO film, the (100) orientation is also competing with the preferred (002) orientation. Similar results showing dominant (002) peak have already been reported by Walters and

Table 1. Texture coefficient values calculated from XRD patterns for the identified six main peaks.

Film	Diffraction peaks					
	(100)	(002)	(101)	(102)	(110)	(103)
ZnO	1.276	1.433	0.983	0.822	0.965	0.518
TZO	0.902	2.686	0.654	1.14	0.478	0.798
FZO	0.063	2.694	0.0928	0.759	–	1.008
TFZO	0.880	2.318	0.743	1.177	0.692	0.985

© 2024 The Authors. ChemPlusChem published by Wiley-VCH GmbH

21926506, 0, Downloaded from https://chemistry-europe.onlinelibrary.wiley.com/doi/10.1002/cplu.202400073 by University College London UCL Library Services, Wiley Online Library on [09/05/2024]. See the Terms and Conditions (https://onlinelibrary.wiley.com/terms-and-conditions) on Wiley Online Library for rules of use; OA articles are governed by the applicable Creative Commons License

Chemistry Europe
European Chemical Societies Publishing

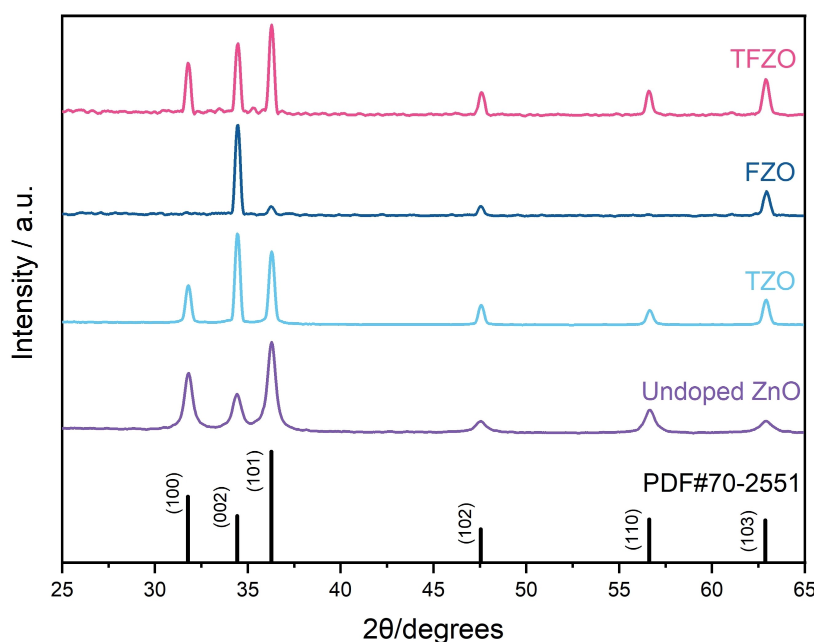

Figure 4. XRD patterns for undoped and doped ZnO films.

Parkin for the doped ZnO films deposited using AACVD.[54] Preferred orientation in the (002) plane has long been reported as a characteristic of ZnO.[54–56]

Preferred orientation of crystallites in case of thin films is associated with the surface free energy of individual crystal plane, and the (002) plane is energetically the most stable plane for ZnO films, regardless the influence of epitaxy.[57]

The average crystallite size (D) is determined through the Scherrer formula,[58] as follows:

$$D = \frac{k\lambda}{\beta cos\theta_B} \quad (2)$$

where k, λ, θ_B and β are the shape factor (0.9), X-ray wavelength (1.5406 Å), Bragg diffraction angle and full width at half maximum (FWHM) of the diffraction peak, respectively. The crystallite diameters, and unit cell parameters are listed in Table 2. The average diameter of crystallites was determined to be in the range of 14–26 nm, in line with the reported results for doped ZnO films.[25] It is evident that the crystallite diameter is increasing with doping which is in line with the reported data and this increase has been assigned to the improved crystal growth with doping.[40] Hence, the sharp peaks produced by doped films indicate a good quality of crystal growth, owing to larger crystallites.[59] This is well-suited for TCOs application as it can reduce scattering at the crystal defects, leading to enhanced carrier properties.[60] However, no direct correlation was identified between the type of dopant and the crystallite diameter.

The unit cell parameters calculated for undoped ZnO film deviates from the standard data, the expanded unit cell volume (0.14%) could be linked to the strain induced by amorphous substrate.[25] The incorporation of dopants led to contraction of unit cell volume compared to the undoped ZnO film which was expected as both Ti^{4+} and F^{-} have smaller ionic radii. As both dopants have almost the same differences in ionic radii (0.06 Å for Ti, 0.07 Å for F) with respect to Zn^{2+}, no large difference was found in their volume contractions.

Surface Morphology

The surface morphologies of the films were determined using scanning electron microscopy (SEM). Figure 5 shows the surface morphologies of undoped and doped ZnO films. The undoped ZnO film is very densely packed, and randomly orientated

Table 2. The unit cell parameters, crystallites diameters and dopant concentrations.

Film	*a*/Å	*c*/Å	Unit cell volume/Å^3	Volume contraction/%	Crystallite diameter/nm	[Ti]/at% (from XPS data)	[F]/at% (from XPS data)
ZnO	3.2511	5.2081	47.67139		14.24		
TZO	3.2461	5.2069	47.51392	0.33	24.30	1.1	
FZO	3.2459	5.2058	47.49803	0.36	24.32		0.9
TFZO	3.2451	5.2013	47.43359	0.49	26.65	0.7	1

© 2024 The Authors. ChemPlusChem published by Wiley-VCH GmbH

21926506, 0, Downloaded from https://chemistry-europe.onlinelibrary.wiley.com/doi/10.1002/cplu.202400073 by University College London UCL Library Services, Wiley Online Library on [09/05/2024]. See the Terms and Conditions (https://onlinelibrary.wiley.com/terms-and-conditions) on Wiley Online Library for rules of use; OA articles are governed by the applicable Creative Commons License

Research Article
doi.org/10.1002/cplu.202400073

21926506, 0, Downloaded from https://chemistry-europe.onlinelibrary.wiley.com/doi/10.1002/cplu.202400073 by University College London UCL Library Services, Wiley Online Library on [09/05/2024]. See the Terms and Conditions (https://onlinelibrary.wiley.com/terms-and-conditions) on Wiley Online Library for rules of use; OA articles are governed by the applicable Creative Commons License

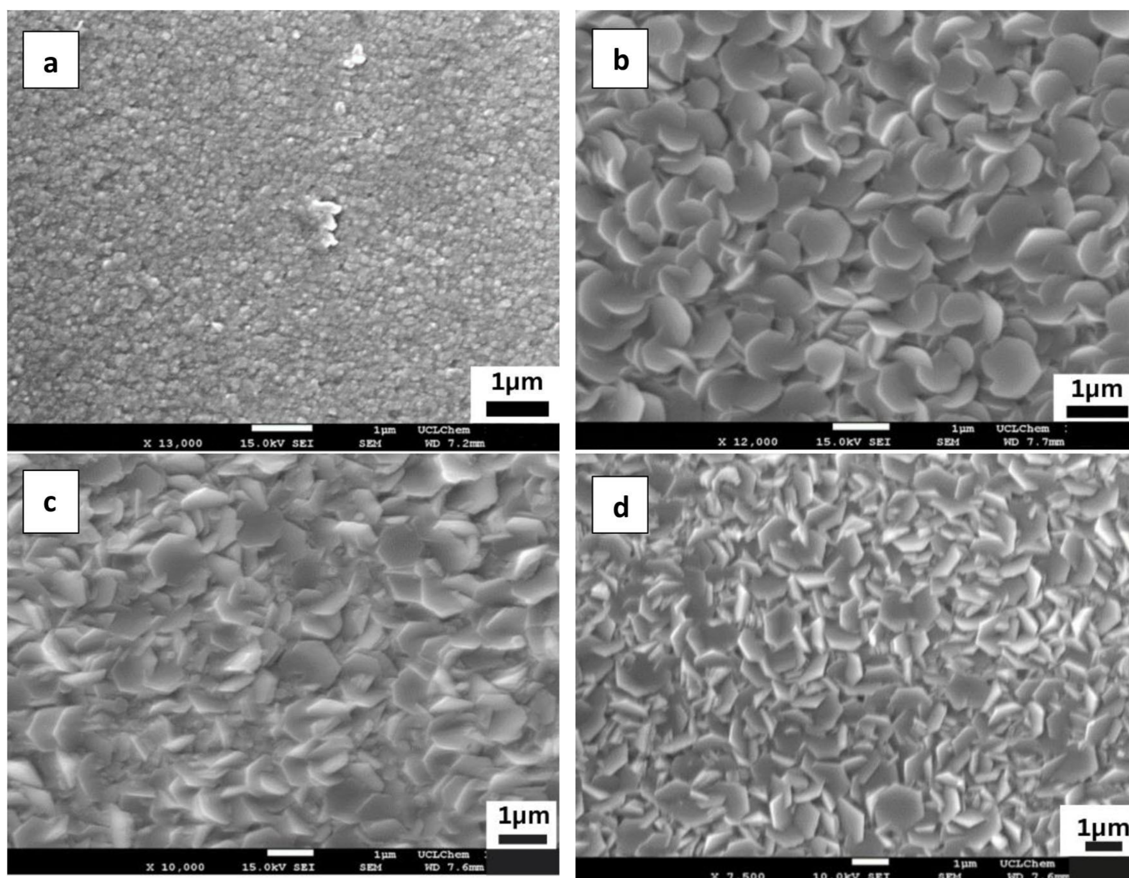

Figure 5. SEM images showing the morphologies of the AACVD deposited a) undoped ZnO, b) TZO, c) FZO, d) TFZO film.

grains in varying sizes, which is somewhat typical of pure ZnO. Similar results have been widely reported for AACVD deposited pure ZnO films.[9,10,18,24,25,40] The addition of dopant(s) had a dramatic effect on the structure, orientation, and grains sizes. The morphologies were fairly consistent, having well-defined grains structures. The grains shapes appeared to be hexagonal and were roughly ~1 μm in diameter. It is evident from Figure 4 that surface morphologies were profoundly dopant dependent. The TZO film displayed well-defined hexagonal features that are randomly oriented upwards and apparently did not have nano-cracks. The incorporation of F impurity in the FZO film resulted in even more densely packed morphology having hexagonal, randomly orientated grains of varying sizes. Most grains in this film showed layer-by-layer growth mechanism, making them more interconnected compared to the grains in TZO film. The co-doped ZnO film showed similar hexagonal, well-connected, and randomly oriented features. The grains of this film seemed to be pristine and smooth, without any apparent morphological defects such as nano-cracks. All the films tend to grow in *c*-direction, which is in line with the XRD results as calculated preferred orientation was found to be in (002) plane. The XRD results coupled with surface morphologies confirm hexagonal structure of doped ZnO films.

The larger grain sizes with well-defined edges and low numbers of defects are generally desired for TCOs as it can minimize the grain boundary scattering which is turn increases the carrier mobility.[61] However, grain boundary scattering is typically assumed to make a minor contribution towards carrier mobility for samples having mean free path of the carriers smaller than the grain size.[62] Meanwhile, grain boundary scattering has a considerably higher impact on ZnO based TCOs compared to ITO.[63] This is linked to the presence of more trap states at the ZnO grain boundaries than ITO.[63,64] Hence, it is important to ensure that doped ZnO has minimum possible morphological defects at the grain structures.

All the doped films showed good quality crystal growth with the well-defined features on the surface. Moreover, these highly textured surface morphologies could be beneficial for TCOs applications such as in solar cells, which requires light scattering to promote light trapping and minimum losses through reflection.[8,9,41,65–68]

Optical Properties

The optical characteristics of the films were analyzed using UV-vis spectroscopy, and the transmittance spectra are plotted in Figure 6. The pure ZnO film showed a transparency of ~79% at 550 nm. This is enhanced up to 85% for TZO and FZO, and up to 87% for TFZO. The average transmittance within the visible spectrum (400-700 nm) increased for doped films FZO and TZO, reaching 83% and 84%, respectively, compared to the 74%

© 2024 The Authors. ChemPlusChem published by Wiley-VCH GmbH

Research Article
doi.org/10.1002/cplu.202400073
Chemistry Europe
European Chemical Societies Publishing

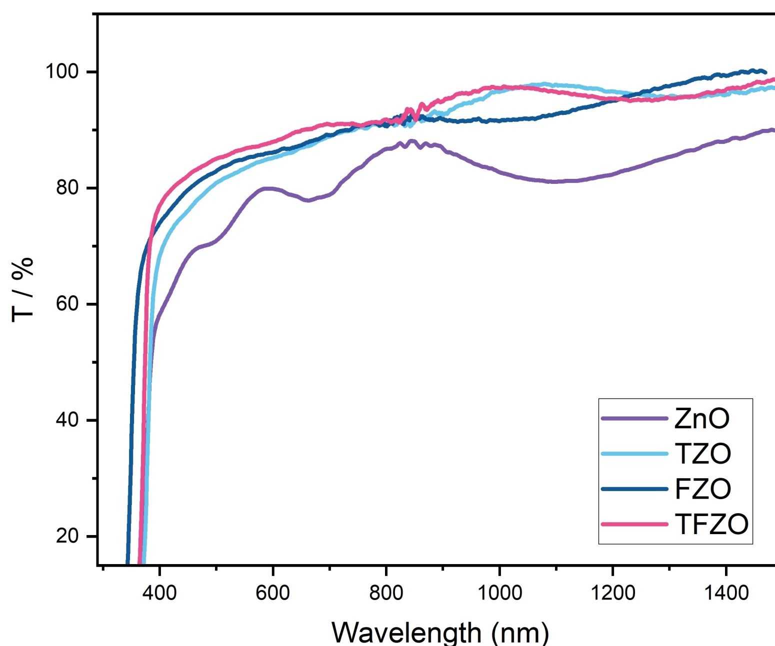

Figure 6. Transmittance spectra of undoped and doped ZnO films.

observed in the undoped ZnO film. Notably, the co-doped film (TFZO) exhibited a further enhancement in average transmittance, achieving a value of 87%. For the doped samples, transmittance was found to increase with wavelength for the measured range. Such a high transmittance across the visible range fulfils the industrial requirement of TCOs.[65,69] The transmittance (~79%) of undoped ZnO film exceeded the films fabricated previously by spray pyrolysis which displayed a transmittance of 50–60% in the visible region and was attributed to high level of carbon contamination.[35] Tauc plot method was employed to determine the band gap values,[70] and are plotted in Figure 7. Undoped ZnO film showed a band gap of 3.27 eV, which increased to 3.48 eV for TZO, 3.51 eV for FZO and 3.60 eV for TFZO. This is in line with the reported results.[10,25] The band gap values of doped ZnO thin films deposited via AACVD are listed in Table 4. The broadening of band gap is assigned to the Moss–Burstein effect, wherein free electrons injected by the dopants occupy the CB which is turn raise the Fermi-level due to increased charge carrier concentration.[3,71] All the states below the Fermi level are fully

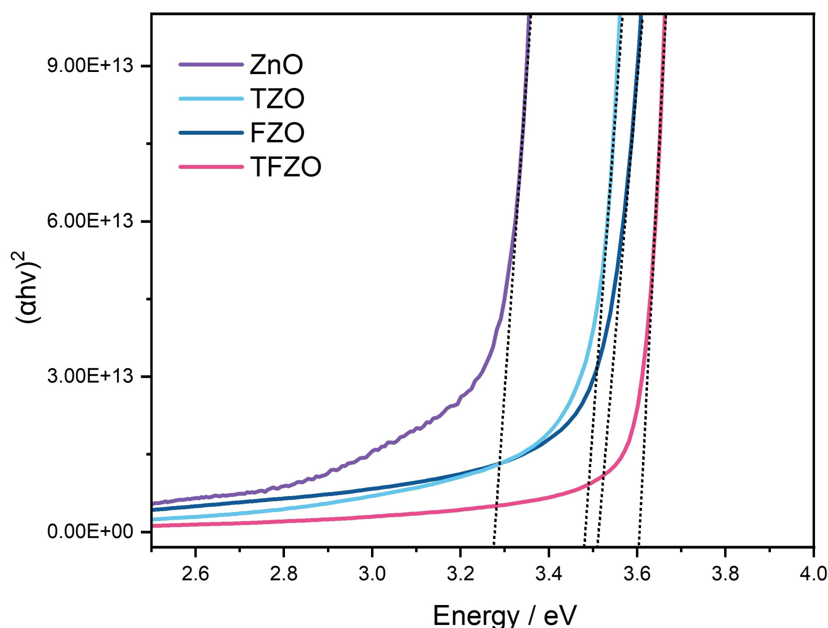

Figure 7. Band gap calculations of undoped and doped ZnO films.

© 2024 The Authors. ChemPlusChem published by Wiley-VCH GmbH

21926506, 0, Downloaded from https://chemistry-europe.onlinelibrary.wiley.com/doi/10.1002/cplu.202400073 by University College London UCL Library Services, Wiley Online Library on [09/05/2024]. See the Terms and Conditions (https://onlinelibrary.wiley.com/terms-and-conditions) on Wiley Online Library for rules of use; OA articles are governed by the applicable Creative Commons License

21926506, 0, Downloaded from https://chemistry-europe.onlinelibrary.wiley.com/doi/10.1002/cplu.202400073 by University College London UCL Library Services, Wiley Online Library on [09/05/2024]. See the Terms and Conditions (https://onlinelibrary.wiley.com/terms-and-conditions) on Wiley Online Library for rules of use; OA articles are governed by the applicable Creative Commons License

occupied, so electrons can be excited only to levels above it. Therefore, the band gap of the doped films increases. However, no particular correlation was found between the optical properties and film thickness.

In addition to the total transmittance, haze value also play a crucial role in the quality of TCO thin films particularly in applications such as touch panels, and displays. The haze value is defined as:

$$\text{Haze value}/\% = \frac{\textit{Diffused Transmittance}}{\textit{Total Transmittance}} \times 100 \quad (3)$$

The haze value of undoped and doped ZnO films were recorded (Figure 8) and found to be less than 5 % for all the films. The TFZO film showed lowest haze value of <0.5 %, which is coupled with high transparency of 87 %.

Electrical Properties

Hall effect measurements were recorded using Van der Pauw technique, at room temperature, shown in Table 3. The negative Hall coefficients displayed the films as n-type. The charge carrier concentration was improved expectedly with Ti or F doping because both dopants are electron donors and thus provide free electrons upon successful substitution. Charge carriers were further increased by co-doping, representing an increase in free carriers. The undoped ZnO film, deposited by using anhydrous zinc acetate, showed high resistivity of 2.13×10^{3} Ω cm. The resistivity value is in line with the reported literature.[72,73] The high resistivity value has been attributed to the porous morphology resulting in low conductivity as pores would impede the electrical conductivity.[73] However, the resistivity value is higher than the reported values of 43 Ω cm[74] and 10 Ω cm.[75] The reasons for this change may be due to the deposition method and the resulting surface morphologies. The high density of extrinsic traps around the grain boundaries would lower the flow of free carriers resulting in high resistivity.[76] In addition, a previous report on AACVD deposited ZnO films claimed that the resistivity values were too high to be measured by Van der Pauw technique.[9] TZO film with the doping concentration of 1.1 at % showed the resistivity value of 1.05×10^{-2} Ω cm; this level of doping has been accounted for optimum conductivity when films were deposited by another method.[32] The lowest mobility of 2.8 $cm^2 V^{-1} s^{-1}$ for this film is in line with the reported values, and this decrease is attributed

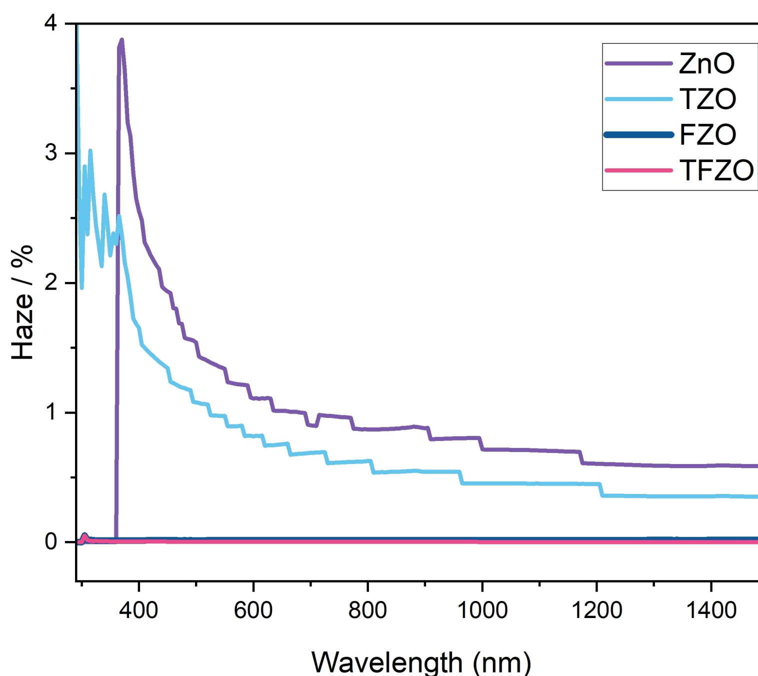

Figure 8. Haze values of undoped and doped ZnO films.

Table 3. Film thickness (d) and Hall effect measurements.

Film	d/nm	n/cm^{-3}	$\mu/cm^2 V^{-1} s^{-1}$	ρ/Ω cm	$Rsh/\Omega cm^{-1}$	ρ/Ω cm (One-year aged films)
ZnO	600	7.56×10^{13}	11.3	2.13×10^{3}	3.55×10^{7}	2.51×10^{3}
Ti:ZnO	630	7.11×10^{18}	2.8	1.05×10^{-2}	1.66×10^{2}	1.04×10^{-2}
F:ZnO	680	6.36×10^{18}	9.7	1.79×10^{-2}	2.63×10^{2}	1.79×10^{-2}
Ti:F:ZnO	650	3.97×10^{20}	8.4	1.69×10^{-3}	26	1.67×10^{-3}

© 2024 The Authors. ChemPlusChem published by Wiley-VCH GmbH

21926506, 0, Downloaded from https://chemistry-europe.onlinelibrary.wiley.com/doi/10.1002/cplu.202400073 by University College London UCL Library Services, Wiley Online Library on [09/05/2024]. See the Terms and Conditions (https://onlinelibrary.wiley.com/terms-and-conditions) on Wiley Online Library for rules of use; OA articles are governed by the applicable Creative Commons License

to lattice distortion, and carrier scattering.[32,77,78] The FZO film with the doping level of 0.9 at% exhibited a resistivity value of 1.79×10^{-2} Ωcm. Previously, a lower resistivity of 10^{-3} and 10^{-4} Ωcm has been reported for 2.0 at%[25] and 1 at%[40] of fluorine, respectively, for F-doped ZnO films deposited by AACVD (Table 4). However, the undoped films in both cases already had resistivity values of the same order of magnitude, hence it was not a dramatic decrease by introducing the impurity. Conversely, this work was able to significantly decrease the resistivity value from 10^{3} (undoped ZnO) to 10^{-3} (TFZO) Ωcm. The FZO film showed higher mobility (9.7 $cm^2 V^{-1} s^{-1}$) than the TZO film (2.8 $cm^2 V^{-1} s^{-1}$), which could be associated to decreased scattering of free carriers by F-dopant.[25,33,34] As anticipated, there was a decrease in mobility with co-doping. The introduction of Ti alongside F reduces the mobility value to 8.4 $cm^2 V^{-1} s^{-1}$. Typically, mobility is controlled by numerous scattering mechanisms, such as ionized scattering of impurity, grain boundary scattering, neutral impurity scattering, and scattering at other dislocations and defects.[79] Furthermore, it was described that mobility is predominantly influenced by the ionized impurity center scattering when charge carrier concentration is very high.[79] In the deposited films, the charge carrier concentration was remarkably high, thus the reduction in mobility could be linked to ionized impurity scattering. The TFZO film has the lowest resistivity of 1.69×10^{-3} Ωcm, which is roughly 6 orders of magnitude less than the undoped film. It is a remarkable decrease in resistivity values compared to the undoped ZnO film than the reported films deposited by the same technique, as listed in Table 4. This fulfils our aim of achieving the enhanced optoelectronic properties by using F as a co-dopant with Ti. The amount of F in the co-doped film stayed approximately the same (1 at%) but the Ti was reduced to 0.70 at%. It is evident that Ti and F doping impurities in the ZnO have increased the carrier concentration along with decreasing the electrical resistance. Doping was found to reduce the sheet resistance, a minimum sheet resistance of 26 Ω

All the films were left in the air for 12 months, washed with common solvents (distilled water, methanol, and ethanol) and the hall effect measurements were remeasured, as shown in Table 3. The films were found to be stable in air over 12 months. The as deposited and one-year aged films also passed the scotch tape test and were not scratchable with stainless steel scalpel and brass stylus.

Conclusions

In summary, undoped ZnO, TZO, FZO, and TFZO films have been synthesized using air stable precursors via AACVD, which is an efficient, reproducible method and allows an easy control over dopant concentration. The dopants were successfully introduced into ZnO to give a pure wurtzite crystal structure, which is confirmed by XRD. XPS analysis confirmed the presence of oxidized dopants in the doped films. The resulting films morphologies analyzed by SEM were fairly consistent,

Table 4. Reported doped ZnO films deposited via AACVD.

Sr.No.	Films	ρ (Ω⁻ cm) (Undoped/Doped)	μ (cm^2/Vs) (Undoped/Doped)	Eg (eV) (Undoped/Doped)	Dopant:Zn (Mole or At%)	Zn-Precursor	Ref.
01	Al:ZnO	$8.18\times10^{0}/1.89\times10^{-2}$	22.5/1.99	3.20/3.34	4.9	$Zn(C_5H_7O_2)_2\cdot2H_2O$	[11]
02	F:ZnO	$5.12\times10^{-4}/3.70\times10^{-4}$	21/32	3.7/3.4	2.0	$ZnEt_2$	[40]
03	F:ZnO Al:ZnO F:Al:ZnO	$2.16\times10^{-3}/1.66\times10^{-3}$ $2.16\times10^{-3}/2.15\times10^{-3}$ $2.16\times10^{-3}/1.85\times10^{-3}$	23.1/12.5 23.1/11.7 23.1/9.7	3.3/3.6 3.3/3.6 3.3/3.7	1.0 1.0 1F:2Al	$ZnEt_2$	[25]
04	Al:ZnO	$4.96\times10^{-2}/3.54\times10^{-3}$	22.92/11.02	3.3/3.4	2.9	$Zn(CH_3COO)_2\cdot2H_2O$	[41]
05	Al:Ga:ZnO In:Ga:ZnO Al:In:ZnO	$NA/1.3\times10^{-2}$ $NA/2.1\times10^{-2}$ $NA/1.6\times10^{-2}$	NA/7.9 NA/3.3 NA/6.8	N/A	9.6Al:4.9Ga 0.9In:8.7Ga 4.2Al:1.8In	$Zn(C_5H_7O_2)_2$	[42]
06	Al:ZnO	$2.8\times10^{-3}/1.96\times10^{-3}$	9.3/10.5	3.7/3.9	7.0	$[Zn(OTf)_2]$	[43]
07	Cl:ZnO	$1.4\times10^{-1}/4.28\times10^{-2}$	4.34/8.66	3.31/3.34	5.0	$Zn(OAc)_2\cdot2H_2O$	[44]
08	Ga:ZnO	$NA/2.3\times10^{-2}$	NA/0.8	NA	5.7	$Zn(C_5H_7O_2)_2\cdot H_2O$	[45]
09	Ga:ZnO	$NA/6.51\times10^{-3}$	NA/3.437	/3.39	3.0	$Zn(C_5H_7O_2)_2\cdot H_2O$	[17]
10	Ga:ZnO	$NA/1.16\times10^{-2}$	25/0.1	3.14/3.37	6.1	$Zn(C_5H_7O_2)_2\cdot H_2O$	[46]
11	Al:ZnO Ga:ZnO	$1.270/2.52\times10^{-1}$ $1.270/7.56\times10^{-1}$	NA NA	3.13/3.25 3.13/3.28	4.8 4.5	$Zn(OC(Me)CHC(Me)N(^iPr))_2]$	[47]
12	Ga:ZnO	$2.14\times10^{-3}/7.8\times10^{-4}$	21.4/18.7	3.25/3.52	5.0	$ZnEt_2$	[8]
13	Ga:ZnO	$11.02\times10^{-3}/4.7\times10^{-4}$	27.4/14.7	3.32/3.86	3.8	$[EtZnO^i Pr]$	[80]
14	Mo:ZnO	$3.7\times10^{-3}/2.6\times10^{-3}$	16.19/10.02	NA	0.57	$ZnEt_2$	[18]
15	P:ZnO	$NA/6.0\times10^{-3}$	NA/6.65	3.28/3.3	6.5	$Zn(OAc)_2\cdot2H_2O$	[20]
16	Si:ZnO	$NA/2.0\times10^{-2}$	NA/16.5	3.16/3.19	4.0	$Zn(acac)_2$	[9]
17	Cl:ZnO	$1.4/2.72\times10^{-3}$	4.34/26.74	3.32/3.30	5.0	$Zn(CH_3COO)_2\cdot2H_2O$	[24]
18	Sc:ZnO	$1.3\times10^{-1}/1.2\times10^{-3}$	2.30/7.50	3.34/3.45	1.0	$Zn(CH_3COO)_2$	[10]
19	B:ZnO	$2.1\times10^{-1}/5.8\times10^{-3}$	NA	NA	7.5	$Zn(CH_3COO)_2\cdot2H_2O$	[81]

© 2024 The Authors. ChemPlusChem published by Wiley-VCH GmbH

21926506, 0, Downloaded from https://chemistry-europe.onlinelibrary.wiley.com/doi/10.1002/cplu.202400073 by University College London UCL Library Services, Wiley Online Library on [09/05/2024]. See the Terms and Conditions (https://onlinelibrary.wiley.com/terms-and-conditions) on Wiley Online Library for rules of use; OA articles are governed by the applicable Creative Commons License

showing hexagonal grains with defined grain boundaries. Co-doping with 0.70 at% titanium and 1 at% fluorine resulted a decrease in resistivity values, reaching a minimum value of 1.69×10^{-3} Ωcm and a sheet resistance of 26 Ω

Supporting Information

The supporting information is available free of charge. It contains additional experimental data on the different concentrations (mol%) of dopant(s) that were used to determine the optimum dopant(s) concentration for this work.

Author Contributions

The manuscript was written through contributions of all authors. All authors have given approval to the final version of the manuscript. All the authors contributed equally.

Acknowledgements

The authors would like to express their sincere gratitude to Dr. Sanjay Sathasivam for his unwavering support and constructive discussions related to Hall effect measurements and spectroscopy measurements. Iqra Ramzan is thankful for the funding received for this research from NSG Pilkington Glass Ltd. and UCL Dean's prize. Part of this work was supported by Engineering and Physical Sciences Research Council (EPSRC) (Grant Number: EP/W010798/1). The authors would also like to thank NSG Pilkington Glass Ltd. for providing glass substrates for research conducted in this work.

Conflict of Interests

The authors declare no conflict of interest.

Data Availability Statement

The data that support the findings of this study are available from the corresponding author upon reasonable request.

Keywords: transparent conducting oxides · Co-doped Zinc oxide · Titanium and Fluorine co-doped Zinc oxide · electronic materials · wide band gap material

[1] K. Ellmer, *Nat. Photonics* **2012**, *6* (12), 809–817. https://doi.org/10.1038/NPHOTON.2012.282.
[2] T. Minami, *Semicond. Sci. Technol.* **2005**, *20* (4), S35. https://doi.org/10.1088/0268-1242/20/4/004.
[3] N. Noor, I. P. Parkin, *J. Mater. Chem. C* **2013**, *1* (5), 984–996. https://doi.org/10.1039/C2TC00400C.
[4] S. Kahraman, H. Çakmak, S. Çetinkaya, F. Bayansal, H. Çetinkara, H. Güder, *J. Cryst. Growth* **2013**, *363*, 86–92. https://doi.org/10.1016/j.jcrysgro.2012.10.018.
[5] A. M. Ganose, D. O. Scanlon, *J. Mater. Chem. C* **2016**, *4* (7), 1467–1475. https://doi.org/10.1039/C5TC04089B.
[6] H. R. Khan, M. Aamir, B. Akram, M. A. Malik, A. A. Tahir, M. A. Choudry, J. Akhtar, *Bull. Mater. Sci.* **2022**, *45* (2), 55.
[7] K. Natu, V. K. Kaushik, M. Laad, *J. Korean Phys. Soc.* **2023**, *83* (3), 200–208.
[8] S. D. Ponja, S. Sathasivam, I. P. Parkin, C. J. Carmalt, *Sci. Rep.* **2020**, *10* (1), 638. https://doi.org/10.1038/s41598-020-57532-7.
[9] D. B. Potter, M. J. Powell, J. A. Darr, I. P. Parkin, C. J. Carmalt, *RSC Adv.* **2017**, *7* (18), 10806–10814. https://doi.org/10.1039/C6RA27748A.
[10] S. C. Dixon, S. Sathasivam, B. A. Williamson, D. O. Scanlon, C. J. Carmalt, I. P. Parkin, *J. Mater. Chem. C* **2017**, *5* (30), 7585–7597. https://doi.org/10.1039/C7TC02389H.
[11] V. K. Kaushik, C. Mukherjee, T. Ganguli, P. Sen, *J. Alloys Compd.* **2016**, *689*, 1028–1036. https://doi.org/10.1016/j.jallcom.2016.08.022.
[12] S. Durrani, E. Khawaja, A. Al-Shukri, M. Al-Kuhaili, *Energy and Buildings* **2004**, *36* (9), 891–898. https://doi.org/10.1016/j.enbuild.2004.02.003.
[13] D. Shao, J. Gao, G. Xin, Y. Wang, L. Li, J. Shi, J. Lian, N. Koratkar, S. Sawyer, *Small* **2015**, *11* (36), 4785–4792. https://doi.org/10.1002/smll.201501411.
[14] M. R. Waugh, G. Hyett, I. P. Parkin, *Chem. Vap. Deposition* **2008**, *14* (11–12), 366–372. https://doi.org/10.1002/cvde.200806718.
[15] A. Kumar, D. K. Gorai, M. I. Ahmad, *J. Mater. Sci. Mater. Electron.* **2023**, *34* (5), 426.
[16] I. R. Cisneros-Contreras, G. López-Ganem, O. Sánchez-Dena, Y. H. Wong, A. L. Pérez-Martínez, A. Rodríguez-Gómez, *Physics* **2023**, *5* (1), 45–58.
[17] S. Chen, N. Noor, I. P. Parkin, R. Binions, *J. Mater. Chem. A* **2014**, *2* (40), 17174–17182. https://doi.org/10.1039/C4TA03888F.
[18] D. Zhao, S. Sathasivam, J. Li, C. J. Carmalt, *ACS Appl. Electron. Mater.* **2019**, *2* (1), 120–125. https://doi.org/10.1021/acsaelm.9b00647.
[19] A. Nebatti, A. Zekri, Y. Zakaria, R. Singh, S. Mukherjee, A. Kadari, M. Guezzoul, K. Khodja, B. Amrani, B. Aïssa, *J. Mol. Struct.* **2023**, *1286*, 135566.
[20] D. Zhao, J. Li, S. Sathasivam, C. J. Carmalt, *RSC Adv.* **2020**, *10* (57), 34527–34533. https://doi.org/10.1039/D0RA05667G.
[21] T. Minami, T. Yamamoto, T. Miyata, *Thin Solid Films* **2000**, *366* (1–2), 63–68. https://doi.org/10.1016/S0040-6090(00)00731-8.
[22] T. Shirahata, T. Kawaharamura, S. Fujita, H. Orita, *Thin Solid Films* **2015**, *597*, 30–38. https://doi.org/10.1016/j.tsf.2015.11.006.
[23] Z.-L. Tseng, P.-C. Kao, C.-S. Yang, Y.-D. Juang, Y.-M. Kuo, S.-Y. Chu, *J. Electrochem. Soc.* **2011**, *158* (5), J133. https://doi.org/10.1149/1.3554730.
[24] A. Jiamprasertboon, S. C. Dixon, S. Sathasivam, M. J. Powell, Y. Lu, T. Siritanon, C. J. Carmalt, *ACS Appl. Electron. Mater.* **2019**, *1* (8), 1408–1417. https://doi.org/10.1021/acsaelm.9b00190.
[25] S. D. Ponja, S. Sathasivam, I. P. Parkin, C. J. Carmalt, *RSC Adv.* **2014**, *4* (91), 49723–49728. https://doi.org/10.1039/C4RA09997D.
[26] Y.-C. Tseng, Y.-J. Lin, H.-C. Chang, Y.-H. Chen, C.-J. Liu, Y.-Y. Zou, *J. Lumin.* **2012**, *132* (2), 491–494. https://doi.org/10.1016/j.jlumin.2011.08.016.
[27] Y.-M. Lu, C.-M. Chang, S.-I. Tsai, T.-S. Wey, *Thin Solid Films* **2004**, *447*: 56–60. https://doi.org/10.1016/j.tsf.2003.09.022.
[28] K. Bergum, P.-A. Hansen, H. Fjellvåg, O. Nilsen, *J. Alloys Compd.* **2014**, *616*, 618–624. https://doi.org/10.1016/j.jallcom.2014.07.177.
[29] Z. Zhong, T. Zhang, *Mater. Lett.* **2013**, *96*, 237–239. https://doi.org/10.1016/j.matlet.2013.01.025.
[30] V. Karpina, V. Lazorenko, C. Lashkarev, V. Dobrowolski, L. Kopylova, V. Baturin, S. Pustovoytov, A. J. Karpenko, S. Eremin, P. Lytvyn, *Cryst. Res. Technol.* **2004**, *39* (11), 980–992. https://doi.org/10.1002/crat.200310283.
[31] E. Muchuweni, T. Sathiaraj, H. Nyakotyo, *Heliyon* **2017**, *3* (4). https://doi.org/10.1016/j.heliyon.2017.e00285.
[32] S.-S. Lin, J.-L. Huang, D.-F. Lii, *Mater. Chem. Phys.* **2005**, *90* (1), 22–30. https://doi.org/10.1016/j.matchemphys.2004.08.040.
[33] H. Xu, Y. Liu, R. Mu, C. Shao, Y. Lu, D. Shen, X. Fan, *Appl. Phys. Lett.* **2005**, *86* (12). https://doi.org/10.1063/1.1884256.
[34] Y.-J. Choi, K.-M. Kang, H.-H. Park, *Sol. Energy Mater. Sol. Cells* **2015**, *132*, 403–409. https://doi.org/10.1016/j.solmat.2014.09.029.
[35] N. Rashidi, V. L. Kuznetsov, J. R. Dilworth, M. Pepper, P. J. Dobson, P. P. Edwards, *J. Mater. Chem. C* **2013**, *1* (42), 6960–6969. https://doi.org/10.1039/C3TC31129E.
[36] R. Sharma, K. Sehrawat, R. Mehra, *Curr. Appl. Phys.* **2010**, *10* (1), 164–170. https://doi.org/10.1016/j.cap.2009.05.013.
[37] C. G. Granqvist, *Sol. Energy Mater. Sol. Cells* **2007**, *91* (17), 1529–1598. https://doi.org/10.1016/j.solmat.2007.04.031.
[38] V. K. Kaushik, T. Ganguli, R. Kumar, C. Mukherjee, P. Sen, *Thin Solid Films* **2012**, *520* (9), 3505–3509. https://doi.org/10.1016/j.tsf.2011.12.075.

© 2024 The Authors. ChemPlusChem published by Wiley-VCH GmbH

21926506, 0, Downloaded from https://chemistry-europe.onlinelibrary.wiley.com/doi/10.1002/cplu.202400073 by University College London UCL Library Services, Wiley Online Library on [09/05/2024]. See the Terms and Conditions (https://onlinelibrary.wiley.com/terms-and-conditions) on Wiley Online Library for rules of use; OA articles are governed by the applicable Creative Commons License

[39] C. E. Knapp, C. J. Carmalt, *Chem. Soc. Rev.* **2016**, *45* (4), 1036–1064. https://doi.org/10.1039/C5CS00651A.

[40] D. S. Bhachu, G. Sankar, I. P. Parkin, *Chem. Mater.* **2012**, *24* (24), 4704–4710. https://doi.org/10.1021/cm302913b.

[41] J. Li, S. Sathasivam, A. Taylor, C. J. Carmalt, I. P. Parkin, *RSC Adv.* **2018**, *8* (74), 42300–42307. https://doi.org/10.1039/C8RA09338E.

[42] D. B. Potter, M. J. Powell, I. P. Parkin, C. J. Carmalt, *J. Mater. Chem. C* **2018**, *6* (3), 588–597. https://doi.org/10.1039/C7TC04003B.

[43] J. A. Manzi, C. E. Knapp, I. P. Parkin, C. J. Carmalt, *Thin Solid Films* **2016**, *616*, 477–481. https://doi.org/10.1016/j.tsf.2016.09.008.

[44] A. Jiamprasertboon, M. J. Powell, S. C. Dixon, R. Quesada-Cabrera, A. M. Alotaibi, Y. Lu, A. Zhuang, S. Sathasivam, T. Siritanon, I. P. Parkin, *J. Mater. Chem. A* **2018**, *6* (26), 12682–12692. https://doi.org/10.1039/C8TA01420E.

[45] S. Chen, G. Carraro, D. Barreca, R. Binions, *Thin Solid Films* **2015**, *584*, 316–319. https://doi.org/10.1016/j.tsf.2014.11.092.

[46] S. Chen, G. Carraro, D. Barreca, A. Sapelkin, W. Chen, X. Huang, Q. Cheng, F. Zhang, R. Binions, *J. Mater. Chem. A* **2015**, *3* (24), 13039–13049. https://doi.org/10.1039/C5TA02163D.

[47] C. E. Knapp, C. Dyer, N. P. Chadwick, R. Hazael, C. J. Carmalt, *Polyhedron* **2018**, *140*, 35–41. https://doi.org/10.1016/j.poly.2017.10.036.

[48] S. Karamat, R. Rawat, P. Lee, T. Tan, R. Ramanujan, *Prog. Nat. Sci.* **2014**, *24* (2), 142–149. https://doi.org/10.1016/j.pnsc.2014.03.009.

[49] X. Wang, F. Zhang, Z. Zheng, L. Chen, H. Wang, C. Li, X. Lui, *Thin Solid Films* **2000**, *365* (1), 94–98. https://doi.org/10.1016/S0040-6090(99)-01082-2.

[50] R. Zanoni, G. Righini, A. Montenero, G. Gnappi, G. Montesperelli, E. Traversa, G. Gusmano, *Surf. Interface Anal.* **1994**, *22* (1–12), 376–379. https://doi.org/10.1002/sia.740220182.

[51] X. Noirfalise, T. Godfroid, G. Guisbiers, R. Snyders, *Acta Mater.* **2011**, *59* (20), 7521–7529. https://doi.org/10.1016/j.actamat.2011.07.068.

[52] B. Dzhurinskii, D. Gati, N. Sergushin, V. Nefedov, Y. V. Salyn, *Russ. J. Inorg. Chem.* **1975**, *20*, 2307–2314.

[53] D. P. Joseph, M. Saravanan, B. Muthuraaman, P. Renugambal, S. Sambasivam, S. P. Raja, P. Maruthamuthu, C. Venkateswaran, *Nanotechnology* **2008**, *19* (48), 485707.

[54] G. Walters, I. Parkin, *Appl. Surf. Sci.* **2009**, *255* (13–14), 6555–6560. https://doi.org/10.1016/j.apsusc.2009.02.039.

[55] A. Babar, P. Deshamukh, R. Deokate, D. Haranath, C. Bhosale, K. Rajpure, *J. Phys. D* **2008**, *41* (13), 135404. https://doi.org/10.1088/0022-3727/41/13/135404.

[56] A. Douayar, R. Diaz, F. C. El Moursli, G. Schmerber, A. Dinia, M. Abd-Lefdil, *Eur. Phys. J. Appl. Phys.* **2011**, *53* (2), 20501. https://doi.org/10.1051/epjap/2010100364.

[57] N. Fujimura, T. Nishihara, S. Goto, J. Xu, T. Ito, *J. Cryst. Growth* **1993**, *130* (1–2), 269–279. https://doi.org/10.1016/0022-0248(93)90861-P.

[58] B. D. Cullity, Addison-Wesley Publishing, **1956**.

[59] M. A. Ehsan, H. N. Ming, M. Misran, Z. Arifin, E. R. Tiekink, A. P. Safwan, M. Ebadi, W. J. Basirun, M. Mazhar, *Chem. Vap. Deposition* **2012**, *18* (7–9), 191–200. https://doi.org/10.1002/cvde.201206988.

[60] M. Ohyama, H. Kozuka, T. Yoko, *J. Am. Ceram. Soc.* **1998**, *81* (6), 1622–1632. https://doi.org/10.1111/j.1151-2916.1998.tb02524.X.

[61] H.-W. Wu, R.-Y. Yang, C.-M. Hsiung, C.-H. Chu, *Thin Solid Films* **2012**, *520* (24), 7147–7152. https://doi.org/10.1016/j.tsf.2012.07.124.

[62] K. Saw, N. Aznan, F. Yam, S. Ng, S. Pung, *PLoS One* **2015**, *10* (10), e0141180. https://doi.org/10.1371/journal.pone.0141180.

[63] H. Liu, V. Avrutin, N. Izyumskaya, Ü. Özgür, H. Morkoç, *Superlattices Microstruct.* **2010**, *48* (5), 458–484. https://doi.org/10.1016/j.spmi.2010.08.011.

[64] K. Ellmer, R. Mientus, *Thin Solid Films* **2008**, *516* (17), 5829–5835. https://doi.org/10.1016/j.tsf.2007.10.082.

[65] D. S. Bhachu, M. R. Waugh, K. Zeissler, W. R. Branford, I. P. Parkin, *Chem. A Eur. J.* **2011**, *17* (41), 11613–11621. https://doi.org/10.1002/chem.201100399.

[66] T. Minami, *MRS Bull.* **2000**, *25* (8), 38–44. https://doi.org/10.1557/mrs2000.149.

[67] D. B. Potter, D. S. Bhachu, M. J. Powell, J. A. Darr, I. P. Parkin, C. J. Carmalt, *Phys. Status Solidi A* **2016**, *213* (5), 1346–1352.

[68] D. B. Potter, I. P. Parkin, C. J. Carmalt, *RSC Adv.* **2018**, *8* (58), 33164–33173.

[69] X. Hou, K. L. Choy, *Chem. Vap. Deposition* **2006**, *12* (10), 583–596. https://doi.org/10.1002/cvde.200600033.

[70] J. Tauc, *Mater. Res. Bull.* **1968**, *3* (1), 37–46. https://doi.org/10.1016/0025-5408(68)90023-8.

[71] M. A. Mohaseba, A. A. Aboud, *J. Mater. Sci. Mater. Electron.* **2023**, *34* (11), 941.

[72] E. Bacaksiz, M. Parlak, M. Tomakin, A. Özçelik, M. Karakız, M. Altunbaş, *J. Alloys Compd.* **2008**, *466* (1–2), 447–450. https://doi.org/10.1016/j.jallcom.2007.11.061.

[73] M. Çopuroğlu, L. H. K. Koh, S. O'Brien, G. M. Crean, *J. Sol-Gel Sci. Technol.* **2009**, *52*, 432–438. https://doi.org/10.1007/s10971-009-2016-0.

[74] M. Mohammad, A. Hashim, M. Al-Maamory, *Mater. Chem. Phys.* **2006**, *99* (2–3), 382–387. https://doi.org/10.1016/j.matchemphys.2005.11.009.

[75] Y. Ohya, H. Saiki, Y. Takahashi, *J. Mater. Sci.* **1994**, *29*, 4099–4103. https://doi.org/10.1007/BF00355977.

[76] J. Sun, T. Yang, G. Du, H. Liang, J. Bian, L. Hu, *Appl. Surf. Sci.* **2006**, *253* (4), 2066–2070. https://doi.org/10.1016/j.apsusc.2006.03.092.

[77] J.-C. Lin, M.-C. Huang, T. Wang, J.-N. Wu, Y.-T. Tseng, K.-C. Peng, *Mater. Express* **2015**, *5* (2), 153–158. https://doi.org/10.1166/mex.2015.1218.

[78] Z.-Y. Ye, H.-L. Lu, Y. Geng, Y.-Z. Gu, Z.-Y. Xie, Y. Zhang, Q.-Q. Sun, S.-J. Ding, D. W. Zhang, *Nanoscale Res. Lett.* **2013**, *8*: 1–6. https://doi.org/10.1186/1556-276X-8-108.

[79] G. Sanon, R. Rup, A. Mansingh, *Thin Solid Films* **1990**, *190* (2), 287–301. https://doi.org/10.1016/0040-6090(89)90918-8.

[80] C. Sanchez-Perez, S. C. Dixon, J. A. Darr, I. P. Parkin, C. J. Carmalt, *Chem. Sci.* **2020**, *11* (19), 4980–4990. https://doi.org/10.1039/D0SC00502A.

[81] D. Zhao, S. Sathasivam, M. Wang, C. J. Carmalt, *RSC Adv.* **2022**, *12* (51), 33049–33055.

Manuscript received: January 26, 2024
Revised manuscript received: March 31, 2024
Accepted manuscript online: April 9, 2024
Version of record online: ■■, ■■

© 2024 The Authors. ChemPlusChem published by Wiley-VCH GmbH

RESEARCH ARTICLE

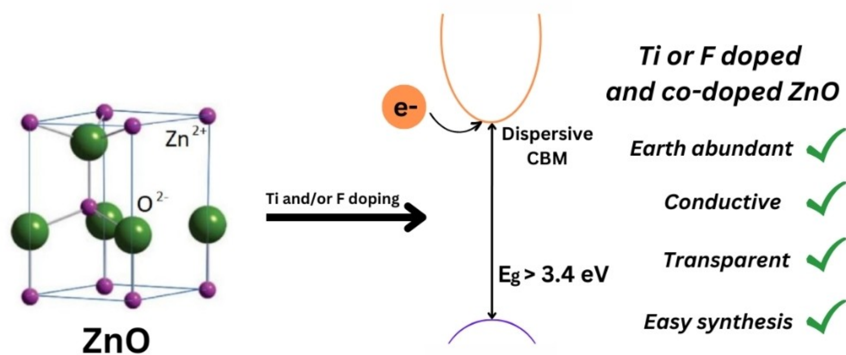

Enhanced electrical and optical properties of transparent conductive titanium and fluorine co-doped zinc oxide films. This research investigates the synthesis and characterization of Ti and F co-doped ZnO films, highlighting their potential for transparent electronics and optoelectronic devices.

*I. Ramzan, J. Borowiec, I. P. Parkin, C. J. Carmalt**

1 – 12

Transparent Conductive Titanium and Fluorine Co-doped Zinc Oxide Films

21926506, 0, Downloaded from https://chemistry-europe.onlinelibrary.wiley.com/doi/10.1002/cplu.202400073 by University College London UCL Library Services, Wiley Online Library on [09/05/2024]. See the Terms and Conditions (https://onlinelibrary.wiley.com/terms-and-conditions) on Wiley Online Library for rules of use; OA articles are governed by the applicable Creative Commons License